

PCCP

Accepted Manuscript



This is an *Accepted Manuscript*, which has been through the Royal Society of Chemistry peer review process and has been accepted for publication.

Accepted Manuscripts are published online shortly after acceptance, before technical editing, formatting and proof reading. Using this free service, authors can make their results available to the community, in citable form, before we publish the edited article. We will replace this *Accepted Manuscript* with the edited and formatted *Advance Article* as soon as it is available.

You can find more information about *Accepted Manuscripts* in the [Information for Authors](#).

Please note that technical editing may introduce minor changes to the text and/or graphics, which may alter content. The journal's standard [Terms & Conditions](#) and the [Ethical guidelines](#) still apply. In no event shall the Royal Society of Chemistry be held responsible for any errors or omissions in this *Accepted Manuscript* or any consequences arising from the use of any information it contains.

Asymmetric bi-layer PFSA membranes as model systems for the study of water management in the PEMFC

Cite this: DOI: 10.1039/x0xx00000x

A Z. Peng,^{a,b} A. Morin,^{*a} P. Huguet,^b Y. Lanteri,^b and S. Deabate^{*b}

Received 00th January 2012,
Accepted 00th January 2012

DOI: 10.1039/x0xx00000x

www.rsc.org/

New bi-layer PFSA membranes made of Nafion® NRE212 and Aquivion™ E79-05s with different equivalent weights are prepared with the aim of managing water repartition in the PEMFC. The membrane water transport properties, *i.e.* back-diffusion and electroosmosis, as well as the electrochemical performances are compared to those of state-of-art materials. The actual water content (inner water concentration profile across the membrane thickness) is measured under operation in the fuel cell by *in situ* Raman microspectroscopy. The orientation of the equivalent weight gradient with respect to the water external gradient and to the proton flow direction affects the membrane water content, the water transport ability and, thus, the fuel cell performances. Higher power outputs, related to lower ohmic losses, are observed when the membrane is assembled with the lower equivalent weight layer (Aquivion™) at the anode side. This orientation, corresponding to enhanced water transport by back-flow while electroosmosis remains unaffected, results in the higher hydration of the membrane and of the anode active layer during operation. Also, polarization data suggest a different water repartition in the fuel cell along the on-plane direction. Even if the interest of multi-layer PFSA membranes as perspective electrolytes for PEMFCs is not definitively attested, these materials appear excellent model systems to establish relationships between the membrane transport properties, the water distribution in the fuel cell and the electrochemical performances. Thanks to the micrometric resolution, *in situ* Raman microspectroscopy proves to be a unique tool to measure the actual hydration of the membrane at the surface swept by the hydrated feed gases during operation, so that it can be used as a local probe of the water concentration evolution along the gas distribution channels according to changing working conditions.

1 Introduction

Proton exchange membrane fuel cells (PEMFCs) are considered as one of the most promising opportunities in the field of alternative technologies for environmentally friendly energy generation. An operating PEMFC for commercial use must be able to adapt to variations in power demand and operating conditions while maintaining near optimal performances during several thousands of hours. Current research shows that one of the main issues affecting power output, stability and longevity is the quantity and distribution of water in the system.¹⁻⁶ Actually, the water management is a major engineering challenge for PEMFCs. On one hand, excess water can flood the gas feed channels and the active layers (ALs), hindering mass transport of the reactive gases to catalyst sites and, thus, decreasing the redox reaction rate *i.e.* the current delivered by the FC. Furtehr, long-term flooding accelerates corrosion of the various components of the membrane-electrode

assembly (MEA). More particularly, the platinum of the catalysts particles dissolves and diffuses into the membrane causing irreversible performance losses. On the other hand, insufficient water dehydrates the perfluorosulfonic acid (PFSA) ionomer used to bind the catalyst nanoparticles in the ALs and constituting the membrane, so decreasing the proton current. Therefore, dry cell operation is affected by ohmic losses and, over a long time, causes irreversible damage due to chemical and mechanical degradations of the ionic conductive phase.

Water distribution within the MEA depends on several interrelated factors, among which a key one is the membrane transport properties. Two main water transport mechanisms occur across the membrane thickness: electroosmosis, where water is dragged by protons as H_3O^+ from the anode to the cathode, and back-flow, induced by the different activities of water at the opposite sides of the membrane. The net overall water cross-flow is typically assumed as the linear superposition of these transport mechanisms. Electroosmosis is

usually considered to induce unfavourable dehydration of both the membrane and the electrode at the anode side, particularly when high current intensities are delivered by the PEMFC.⁷⁻¹⁵ Back-flow, related to the electrochemical production of water at the cathode, should have the beneficial effect to offset electroosmosis and, thus, balance the water distribution between anode and cathode.¹⁶⁻¹⁹

One of the usual approaches for managing water distribution inside the MEA is to develop new membranes with less marked dependence of conductivity on hydration, the ultimate aim being to operate the FC with dry feed gases.^{20,21} But, even if many significant advances have been achieved in this field during the last decades, it should be recognized that such alternative materials still exhibit perceived drawbacks, especially in terms of longevity. This causes the PFSA ionomers to remain the state-of-art electrolyte in the PEMFC technology.

An alternative, much less investigated strategy to improve water management is to use current membranes to develop anisotropic multilayer structures with modified water transport properties *i.e.* increased water back-flow and/or limited electroosmosis. Marrony *et al.* first reported about multi-layer membranes consisting in hydrocarbon materials with different ionic exchange capacities (IEC), prepared by successive casting steps.²² Water balance measurements carried out during FC tests with bi-layer sPEEK suggested that the direction of larger water production can be reversed by reversing the membrane orientation in the MEA. Better performances were observed when the higher IEC side was oriented towards the anode. Then, later studies on multi-layer membranes dealt with the development of hybrid or composite materials intended to exhibit improved mechanical properties and proton conductivity,^{23,24} oxidative stability²⁵ or decreased methanol crossover.^{26,27} Only recently, Woo *et al.*²⁸ reported anew about water management improving by composite membranes with asymmetric structure. So far, the elaboration and the characterization of water transport properties of multi-layer membranes entirely based on PFSA materials have not been particularly investigated.

Systematic approach and final validation of the multilayer strategy first requires investigating model (simpler) materials, in order to establish the actual effect of compositional gradients on water transport. In this context, this work presents the characterization of a new bi-layer membrane readily prepared by hot-compression of commercial PFSA materials, Nafion[®] NRE212 and Aquivion[™] E79-05s, with different IEC and water sorption ability. Nafion[®] is the benchmark long side chain material for PEMFCs. The short side chain Aquivion[™] has recently gained interest as a replacement to Nafion[®] because it has been shown to outperform in operating FC.²⁹⁻³² In this paper, we first report the performances of the FC containing the asymmetric Aquivion/Nafion membrane and operating under representative conditions, as to attest the actual impact of the bi-layer orientation in the MEA. Then, water flows crossing the membrane under electric or water activity gradients are investigated independently, by macroscopic

measurements still carried out as a function of the bi-layer arrangement with respect to the direction of the water transport driving force. Also, measurements are carried out at different relative humidities (RH), since water transport ability and mechanisms are expected to change drastically as a function of the hydration state of the non-crosslinked PFSA ionomer.³³⁻³⁵ Finally, *operando* depth-resolved μ -Raman measurements are used to characterize the evolution of the local membrane water content with the FC working regime.³⁶⁻³⁹ This technique is currently gaining relevance as a unique tool for the measurements of mass transfer profiles of molecular species diffusing or migrating across transparent polymer films.^{40,41} The overall results allow us to go deeper into the knowledge of relationships existing between the membrane hydration state, the water transport ability and fundamental mechanisms, the water distribution in the FC and the performances of the electrochemical system.

2 Experimental

2.1 Membranes

Bi-layers membranes are obtained by hot-compression of Nafion[®] NRE212 (EW = 1100 g/mol, thickness = 50 μ m, purchased from DuPont De Nemours) and Aquivion[™] E79-05s (EW = 790 g/mol, thickness = 50 μ m, from Solvay Specialty Polymers), used as received. The two membranes are first stacked together and maintained under 0.05 MPa compression at 170[°] C for 150 s. Then, compression is increased to 3.5 MPa during 210 s, at the same temperature. Once back at room temperature, the bi-layer is cleaned according to a common procedure that consists in immersion in a 30% wt. HNO₃ solution and stirring during 4 h at room temperature, followed by rinsing with distilled water.

The hot-compression conditions reported here above have been optimized in order to avoid the peeling-off at the interface between the two membranes. The temperature is a key parameter, which has to be higher than the temperature of the mechanical relaxation of Aquivion (the last being higher than that of Nafion). The integrity of the contact interface is checked by submitting the bilayers to several, subsequent dehydration and hydration steps in water at 80[°]C. The effective cohesion at the micrometer scale is confirmed by Raman microspectroscopy. Depth-resolved measurements are carried out at several areas of the bi-layer surface. No loss of the polymer phase spectral signal or presence of water pockets is observed at the interface.

2.2 PEMFC performance measurements

PEMFC tests are carried out with the single cell fixture reported in Fig. 1, having single serpentine gas distribution channels machined in graphite monopolar plates. The rib and channel widths are respectively 0.8 mm and 1.4 mm. MEAs are done by hot-compression (3.5 MPa and 135 [°]C, during 210 s) of the bi-layer membrane within commercial electrodes Johnson Matthey

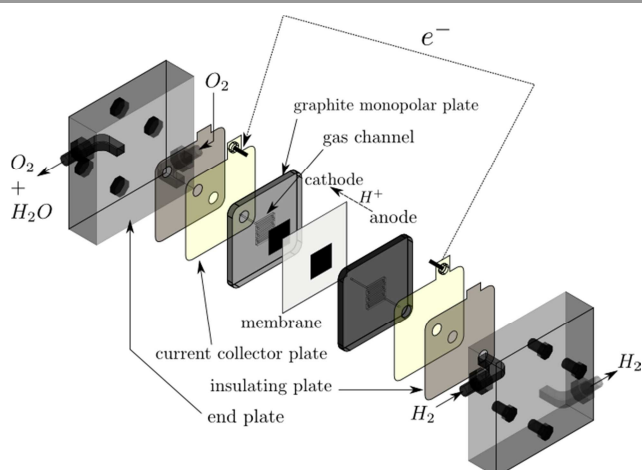


Fig. 1 Schematic representation of the single cell test fixture used for PEMFC tests.

on Toray paper TGP-H-060 (0.4 mg cm⁻² Pt). The active area is 25 cm². on Toray paper TGP-H-060 (0.4 mg cm⁻² Pt).

The FC is operated in the galvanostatic mode, by a potentiostat/galvanostat impedancemeter VSP associated with a 20V/20A VMP@2B booster from Bio-Logic SAS. A Biologic FCT-50S test bench is used to manage the cell temperature, gas flows, pressures and RHs at the inlets. RH is adjusted by passing the dry gas through heated bubble chambers. Gas lines are heated at 120 °C to avoid condensation. Feed gases, supplied in the counter-flow mode, are pure H₂ and O₂ at 1.5 bars, with H₂/O₂ stoichiometry of 1.2/1.5 respectively.

The polarization curves are recorded by sweeping current from 0 up to 1400 mA cm⁻² (value beyond which a steady potential can no longer be attained) at 20 mA s⁻¹. *In situ* EIS is carried out simultaneously, according to a measure for each current increment of 100 mA cm⁻². The investigated frequency range is 0.1 Hz-10 kHz, with 10 points per decade after 4 periods of stabilization. Values are averaged on 4 periods. The ohmic resistance of the MEA is ascribed to the modulus of the complex impedance at the higher frequencies for which the imaginary part reaches zero. Resistances others than ohmic are evaluated by subtracting the ohmic to the overall resistance.

2.3 Sorption Isotherms

The water content at equilibrium of as-received Nafion[®] NRE212 and Aquivion[™] E790-05s membranes is determined for different water activities by the gravimetric method, using a Symmetrical Gravimetric Analyzer SGA-100 equipped with a microbalance and a dew point analyser. Samples are first dried out during 240 min at 60° C under dry N_{2(g)} flow, until the weight loss is lower than 0.001 wt% in 10 min. Then, sorption measurements are carried out at room temperature, using a humidified nitrogen feed to increase the RH from 5 to 95%, per step of 5%.

2.4 Electroosmotic drag measurements

Electroosmotic water flows are usually characterized by the measurement of the K_{drag} coefficient *i.e.* the average number of

water molecules dragged per proton migrating under the electrical gradient. The appropriate method to measure K_{drag} has been comprehensively discussed in a previous study.¹⁴ In this work, electroosmotic measurements are carried out using the same experimental set-up described above (Fig. 1), but with electrodes with lower active area *i.e.* 5 cm². The cell is operated at ambient conditions, in the H₂ pump mode *i.e.* hydrogen is oxidized at the anode and the so-generated protons migrate through the membrane to be reduced at the cathode and give back H₂. The cell set-up has the cathode outlet directly connected to the anode inlet located on the opposite side (Fig. 2), so as both sides of the MEA are in contact with a single gas flow. This allows the water concentration at no-current conditions to be the same at each point of the gas flow on the opposite sides of the membrane, so as to minimize the presence of transverse water concentration gradients *i.e.* parasitic water flows which may affect the accurate measurement of K_{drag} . Hydrogen flow (500 N mL min⁻¹) and stoichiometry (550) are chosen so that the contribution to the overall flow from the hydrogen produced at the cathode or consumed at the anode is negligible. The amount of water dragged by electroosmosis is much lower than the inlet water flow and the RH difference between inlet and outlet at each electrode is minimized ($\Delta\text{RH} \leq 5\%$). The cell is operated galvanostatically at $I = 24 \text{ mA cm}^{-2}$, in order to maintain high stoichiometry and a cell voltage below 1 V (avoiding water electrolysis and/or carbon corrosion). In order to carry out measurements at the steady state, the MEA hydration is monitored by *in situ* EIS (carried out as described above). The typical equilibrating time, corresponding to the time needed for the measured resistance to steady, is $\sim 2 \text{ min}$ and $\sim 1 \text{ h } 30 \text{ min}$ at $I = 24$ and 0 mA cm^{-2} , respectively.

The electroosmotic drag coefficient is calculated for different membrane hydration states, as follows. The starting data are the difference between the RHs measured with and without imposed current, by the gas concentration sensor Piezocon[®] (Lorex Industries, Inc) placed between the anode inlet and the cathode outlet (Fig. 2). At no-current conditions, the water molar fraction $\alpha^{j=0}$ is identical in the whole set-up and related to the inlet water flow $\phi_{\text{H}_2\text{O}}^{\text{inlet}}$, according to:

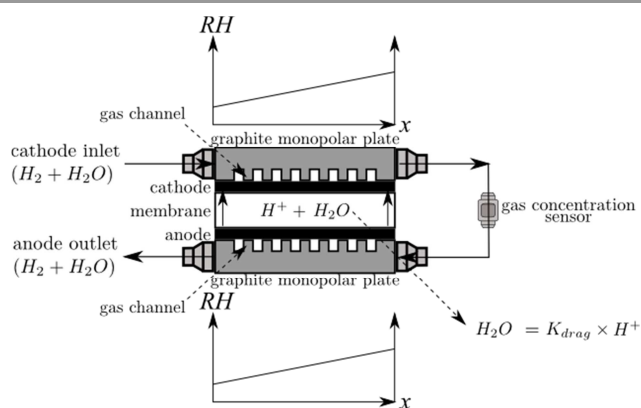


Fig. 2 Schematic representation of the experimental set-up for the measurement of the electroosmotic drag coefficient.

$$\alpha^{i=0} = \frac{\phi_{H_2O}^{inlet}}{\phi_{H_2O}^{inlet} + \phi_{H_2}} \Rightarrow \phi_{H_2O}^{inlet} = \frac{\alpha^{i=0}}{1 - \alpha^{i=0}} \times \phi_{H_2} = \phi_{H_2O}^{i=0} \quad (1)$$

where flows are in mol s^{-1} . Under homogeneous RH conditions, $\phi_{H_2O}^{inlet}$ can be obtained by measuring the water molar fraction at the cathode outlet, knowing the inlet hydrogen flow ϕ_{H_2} . Once $\alpha^{j=0}$ measured, the current I is applied and the water concentration at the cathode outlet increases due to the electroosmotic drag. When a steady state is reached, the value of $\alpha^{j \neq 0}$ is constant and the electroosmotic drag coefficient can be calculated according to:

$$\alpha^{j \neq 0} = \frac{\phi_{H_2O}^{inlet} + \phi_{drag}}{\phi_{H_2O}^{inlet} + \phi_{drag} + \phi_{H_2} + \frac{I}{2 \times N_A \times e^-}} \quad (2)$$

$$\Rightarrow \phi_{drag} = \frac{\alpha^{j \neq 0}}{1 - \alpha^{j \neq 0}} \times \left(\phi_{H_2} + \frac{I}{2 \times N_A \times e^-} \right) - \phi_{H_2O}^{inlet} = \phi_{H_2O}^{i \neq 0} - \phi_{H_2O}^{i=0}$$

where N_A is the Avogadro number ($6.022 \times 10^{23} \text{ mol}^{-1}$), e^- the elementary charge ($1.6 \times 10^{-19} \text{ C}$) and ϕ_{drag} the electroosmotic drag flow (mol s^{-1}), which is then equal to the difference between the water flows $\phi_{H_2O}^{j \neq 0}$ and $\phi_{H_2O}^{j=0}$ deduced from the water molar fractions measured at the cathode outlet with and without current I respectively. The term $I/(2 \times N_A \times e^-)$ originates from the hydrogen formation by proton reduction at the cathode.

The electroosmotic drag coefficient can be finally determined according to:

$$K_{drag} = \frac{\phi_{drag}}{\phi_{protons}} = \frac{\phi_{drag}}{N_A \times e^-} \quad (3)$$

2.5 Measurements of water cross-flows at no-current conditions

As for electroosmosis, measurements of water flows crossing the membrane under external water activity gradients are carried out at ambient and steady conditions, the membrane hydration state being monitored by *in situ* EIS. The experimental set-up used is reported in Fig. 3. The cell is the same as for the electroosmotic drag measurements. The membrane, placed alone between the bipolar plates (no active or gas diffusion layers), is submitted to external water concentration gradients by flowing $H_{2(g)}$ ($1000 \text{ NmL min}^{-1}$) with different RHs at the opposite sides of the cell. The co-flow configuration is used and RHs at the inlets are carefully controlled in order to maintain the same average membrane hydration along the gas distribution channel. The water activity gradient or ΔRH between points placed symmetrically at the opposite surfaces of the membrane decreases along the gas flow path (from the inlet to the outlet) but the average transversal RH stays constant. RHs at the inlets are chosen different enough to avoid reversal of the RH gradient across the membrane as gases move towards the outlet *i.e.* the RH at one side stays always higher than that at the other side.

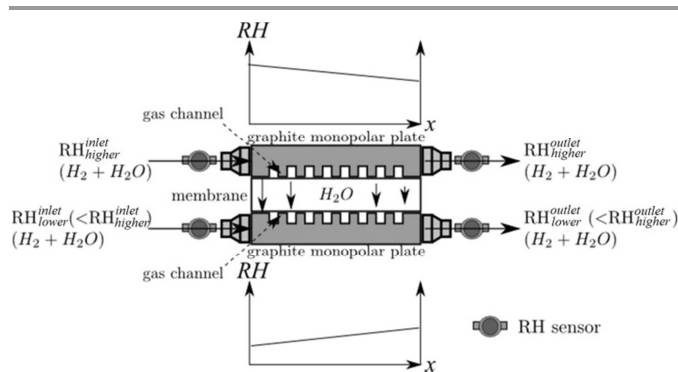


Fig. 3 Schematic representation of the experimental set-up for the measurement of water cross-flows at no-current conditions.

RHs are measured at each inlet and outlet by four Rotronic HygroPalm capacitive sensors, so as to allow water balance measurements for both the cell sides, from which the water cross-flow ϕ_{water} is calculated according to:

$$RH^{inlet} = \frac{\phi^{inlet}}{\phi^{inlet} + \phi_{H_2}} \times \frac{P_{tot}}{P_{vap}^{sat}(T_{cell})} \Rightarrow \phi^{inlet} = \frac{RH^{inlet}}{\frac{P_{tot}}{P_{vap}^{sat}(T_{cell})} - RH^{inlet}} \times \phi_{H_2}$$

$$RH^{outlet} = \frac{\phi^{outlet}}{\phi^{outlet} + \phi_{H_2}} \times \frac{P_{tot}}{P_{vap}^{sat}(T_{cell})} \Rightarrow \phi^{outlet} = \frac{RH^{outlet}}{\frac{P_{tot}}{P_{vap}^{sat}(T_{cell})} - RH^{outlet}} \times \phi_{H_2}$$

$$\phi_{water} = \phi^{inlet} - \phi^{outlet} \quad (4)$$

where ϕ^{inlet} and ϕ^{outlet} are the water flows at the inlet and the outlet, respectively (mol s^{-1}). P_{tot} and $P_{vap}^{sat}(T_{cell})$ correspond to the total pressure of gas flow and the saturation vapour pressure at the cell temperature, respectively (Pa).

The RH from which the $\langle \lambda \rangle$ of the membrane is deduced correspond, here, to the average of the four RH values from the different capacitive sensors of the experimental set-up.

2.6 In situ μ -Raman measurements

The inner water gradient crossing the asymmetric bi-layer membrane under operation is measured by *in situ* Raman microspectroscopy. The principle of the technique, the experimental set-up and the data treatment procedure are presented in detail elsewhere.^{40,41} In short, Raman spectra are accumulated at different depths across the membrane thickness. Once made the appropriate corrections to the raw signal (resumed below and in section 3.3), the amount of water sorbed at each probed position is calculated from the intensity of the related vibrational bands (Fig. S1†).⁴² The specific single cell fixture used, designed in our laboratory,³⁶ is reported in Fig. 4. This cell is made of two 20 mm thick gilded stainless steel monopolar plates with a single machined serpentine gas distribution channel. The depths of the channels are 0.5 and 1.5 mm for the upper (cathode) and lower (anode) plates respectively. The width of the ribs and channels are the same for both plates *i.e.* 1.5 mm. A viewing aperture ($\varnothing 1.2 \text{ mm}$) is

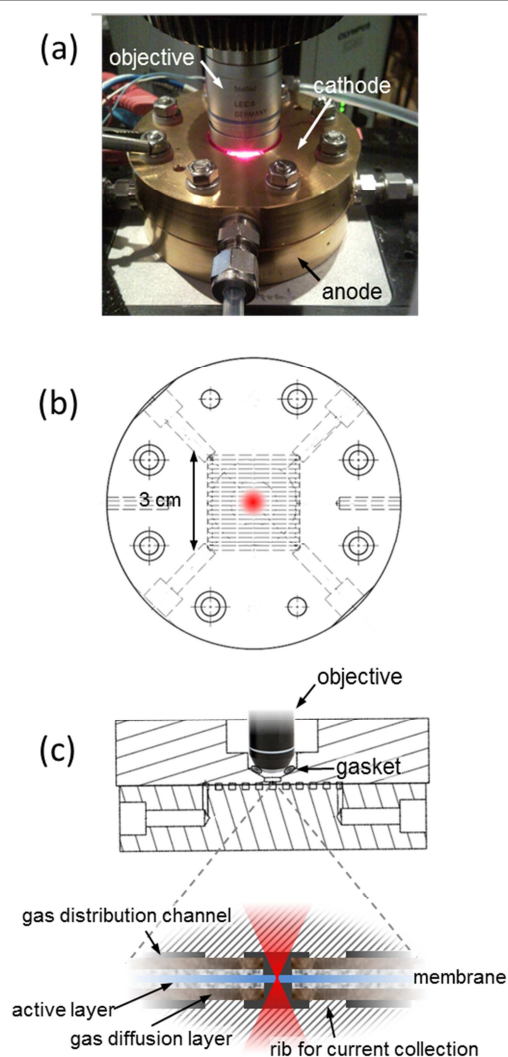


Fig. 4 The PEMFC for in situ Raman analysis: (a) picture during experiment, (b) schematic top view and (c) cross-section.

drilled in the channel in the middle of the active area of the upper gas distribution plate, to provide access of the Raman exciting radiation to the membrane. A compressible gasket, squeezed by the microscope objective, is used to keep the cell tight.

MEAs are assembled as follows. Catalyst coated backing (the same used above) are glued on the gas distribution plates and a hole (\varnothing 400 μm), aligned to the optical pattern, is drilled in each of them. Then, the cell is stacked with the membrane (MEA is compressed to the 70% of the original thickness) and put into oven at 135 $^{\circ}\text{C}$ during 1 h. The electrode active surface is 9 cm^2 . Two bi-layer MEAs are separately mounted and tested, in order to compare the water content profiles for the two possible orientations of the asymmetric membrane.

The FC is operated at ambient conditions of temperature and pressure, using a home-made test bench for gas RH and flow regulation. RH is measured at the inlets with a Rotronic HygroPalm capacitive sensor. Pure H_2/O_2 gases are supplied in

the counter-flow configuration, with constant stoichiometry of 15/60 respectively and 50% RH. These low temperature and high stoichiometry conditions are needed, respectively, to prevent the damage of the microscope objective and to avoid water condensation on the lens. The last is in contact with the cathode feed gas flow and may represent a cold point in the system. During the FC operation, heater mats are used to keep the objective at 38 $^{\circ}\text{C}$ *i.e.* the maximum temperature that can be sustained by the optical device.

Raman spectra are obtained by exciting with the 647.1 nm radiation from an Ar–Kr laser operating at about 100 mW (\sim 40 mW at the sample surface) and recorded with a LABRAM1B confocal Raman spectrometer (Jobin–Yvon S.A., Horiba, France), equipped with a 50X Leica objective (HCX PL Fluotar L 50X/0.55, working distance 8 mm) recovering the backscattered light.

The FC is mounted on an automatic positioning device that allows carrying out spectral measurements at different depths across the membrane cross section. Once steady FC performance is attained, the Raman cartography (\sim 200 spectra, stepping distance 1 μm) is repeated for 12 times to ensure high statistic. The experimental in-depth resolution, measured as previously reported,^{40,41,43} is $7 \pm 1 \mu\text{m}$. The volume of the sample probed by the focalized laser beam at each step of the cartography is $\leq 14 \mu\text{m}^3$. Because of the undesirable fluorescence affecting Raman spectra of fresh membranes, reference water concentration profiles (at no-current conditions) are recorded at the end of the experiment, after a few hours of gas feeding when the inner water content and the MEA resistance (the latter measured by IES as described above) do not change further between two subsequent cartographies. The time needed for one cartography is \sim 1 h.

The local water content of the membrane (volume fraction Φ_V and molecule number $\lambda = [\text{H}_2\text{O}]/[\text{SO}_3]$) is calculated from the ratio between the intensities of the $\nu(\text{O-H})$ mode around 3500 cm^{-1} and some selected Raman bands from the polymer chemical groups, according to:

$$\Phi_V = \frac{V_{\text{H}_2\text{O}}}{V_{\text{H}_2\text{O}} + V_{\text{polymer}}} = \frac{1}{1 + \frac{V_{\text{polymer}}}{V_{\text{H}_2\text{O}}}} = \frac{1}{1 + \beta \times \frac{S_{\text{polymer}}}{S_{\nu(\text{OH})}}} \quad (5)$$

$$\lambda = \frac{V_{\text{H}_2\text{O}} \times \rho_{\text{H}_2\text{O}} \times \text{EW}}{V_{\text{polymer}} \times \rho_{\text{polymer}} \times M_{\text{H}_2\text{O}}} = \frac{\Phi_V \times \rho_{\text{H}_2\text{O}} \times \text{EW}}{(1 - \Phi_V) \times \rho_{\text{polymer}} \times M_{\text{H}_2\text{O}}} \quad (6)$$

where S_{polymer} is the sum of the intensities of the $\nu_s(\text{C-F})$ mode from the polymer backbone (735 cm^{-1}), the $\nu(\text{C-S})$ (675 cm^{-1}) and $\nu(\text{C-F})$ (800 cm^{-1}) vibrations from the pendant chain (Fig. S1 \dagger). As detailed in earlier studies,^{41,42} this calculation procedure represents an effective method to measure the membrane inner water content directly, *i.e.* from the Raman signal of sorbed water, avoiding the need of internal references and minimizing the number of external measurements. The only calibration constant which has to be measured independently is the ratio between the scattering cross-sections of the sorbed water and of the molecular species used for

assessing the ionomer occupation volume $V_{polymer}$ *i.e.* the β coefficient appearing in eqn (5) (for which we refer the reader to Peng *et al.*⁴²). Further, our calculation procedure implies the normalization of the sorbed water by the polymer signal, which allows correcting artificial gradients due to the progressive attenuation of the Raman signal as the probed volume moves deeper into the membrane.^{41,42} Other phenomena which have also to be taken into account in order to recover artefacts-free depth-profiles are the low resolution at the interfaces (due to instrumental spreading)^{43,44} and the artificial shortening of the depth-scale (due to spherical aberrations).⁴⁵ In this work, blurring effects at the interfaces are corrected with a mathematical approach which correlates apparent (raw) and true Raman intensities with the depth-resolution curve of the instrument, the latter measured under the same optical conditions encountered during the *in situ* Raman study. Details can be found in Deabate *et al.*⁴³ and Gallardo *et al.*⁴⁴ Artificial shortening of the depth-scale is corrected by multiplication of the apparent depth-position by the ratio $n = n_1/n_2$ between the refractive index of the membrane ($n_1 = 1.35$) and of the surrounding gas phase ($n_2 = 1.00$). Even if other, more rigorous, mathematical expression can be used (see Everall⁴⁵), our correction represents an effective approximation in the specific case of hydrated PFSA materials and Raman depth-measurements carried out with a confocal set-up.⁴¹

3 Results and discussion

3.1 PEMFC performance

Fig. 5 compares performance data of the FC containing the asymmetric bi-layer membrane, differently oriented in the MEA, to those obtained with symmetric bi-layer materials of the same thickness *i.e.* reference samples consisting of two Nafion or two Aquivion layers stacked together. Measurements have been reproduced at least three times. The observed differences are meaningful and can be reliably ascribed to the membrane and not to changes of the electrodes performances from one assembly to the other. The FC behavior is investigated for two operating conditions of temperature and RH: (i) 60 °C and 100% RH for both gases (“wet” conditions); (ii) 70 °C and 0% RH (“dry”). The heterogeneity of the FC operation (water distribution in the MEA) is expected to increase from “wet” to “dry”.

For both the operating conditions investigated, the different behaviours can be discussed according to two working regimes, namely at low current density, *i.e.* below 600 mA cm⁻², and at high current density *i.e.* above this value. At high current, the FC assembled with the symmetric bi-layer consisting of two identical Aquivion membranes exhibits the best performances while the symmetric bi-layer Nafion/Nafion the worst. The opposite is observed at low current, although the difference is less pronounced. Concerning the asymmetric membrane, better performances are observed when the Aquivion layer is placed at the anode side. It is worth of noting that the behaviour differences between the various symmetric and asymmetric

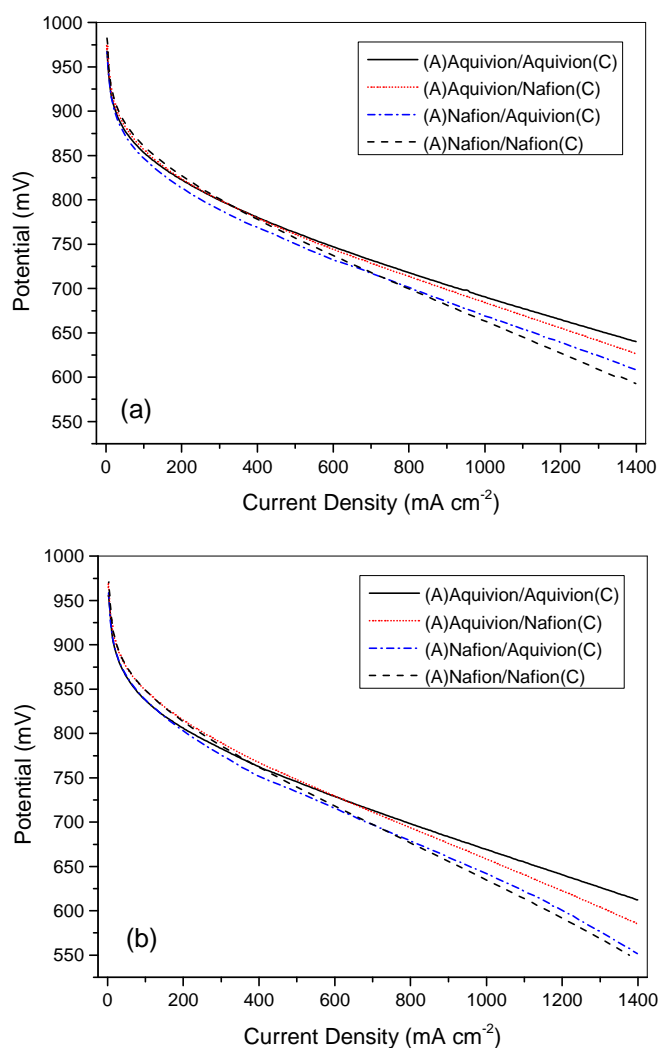


Fig. 5 Fuel cell polarization data: a) 60 °C, 100% RH (“wet” conditions); b) 70 °C, 0% RH (“dry”). H₂/O₂ stoichiometry: 1.2/1.5. In the legend, (A) and (C) denote the anode and the cathode respectively.

materials are enhanced by operating the FC under “dry” conditions (compare Figs. 5a and b), for which back-flow of water from the cathode to the anode is of prime importance to promote hydration of the anode side.

In situ electrochemical impedance spectroscopy (EIS), carried out under dynamic conditions, shows that the different performances observed are strictly related to the FC resistivity, whose major contribution is usually admitted to originate from the PFSA ionomer in the ALs and from the membrane. Fig. 6 reports the evolution of ohmic and non-ohmic (the latter usually referred as “transfer resistance” in literature) contributions to the overall resistivity as a function of the delivered current density. As expected, slightly lower values are measured when the FC is operated under “wet” conditions (Fig. 6a). The decrease of the non-ohmic contributions with the current increase shows that electrode performances as well improve with the increase of the water concentration in the FC.⁴⁶ However, at a given T and RH, the non-ohmic resistivities of

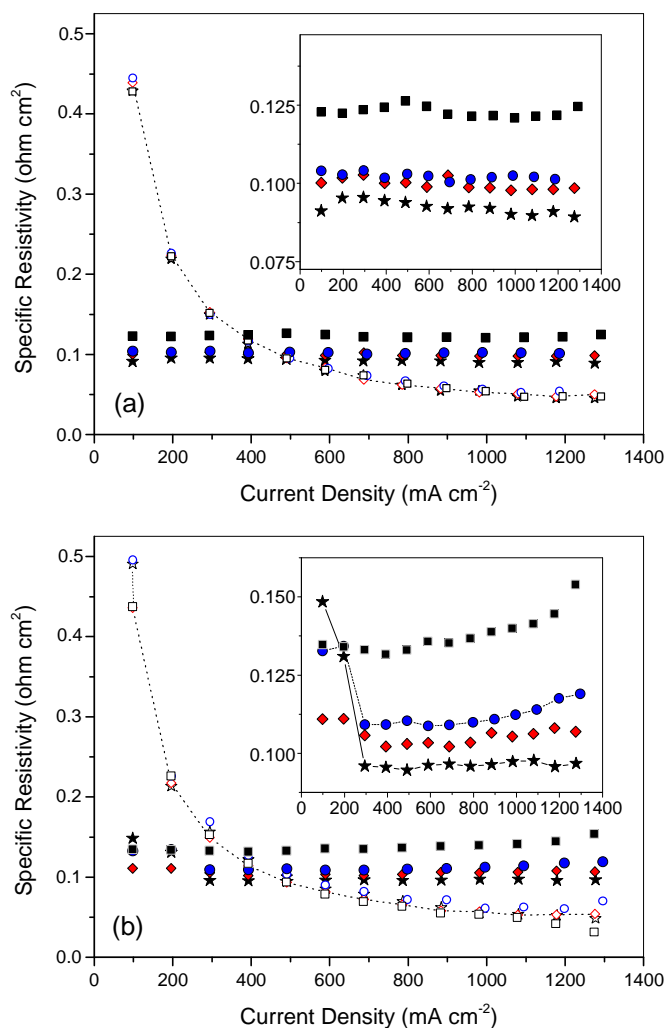


Fig. 6 Specific resistivity obtained from *in situ* EIS measurements as a function of different current densities delivered by the FC. FC operating conditions: (a) 60 °C, 100% RH ("wet"); (b) 70 °C, 0% RH ("dry"). MEAs: (★) (A)Aquivion/Aquivion(C); (◆) (A)Aquivion/Nafion(C); (●) (A)Nafion/Aquivion(C); (■) (A)Nafion/Nafion(C); where (A) and (C) denote the anode and the cathode respectively. Full and open symbols denote ohmic and non-ohmic resistivities, respectively. Insets are magnifications for the detailed view of the ohmic resistivity evolution with current.

the different assemblies are very similar while significant differences can be observed for the ohmic contributions. Ohmic resistivities stay between 0.09 and 0.13 Ω cm² and behave almost constant in the whole investigated current range. A slight increase is observed under "dry" conditions at the higher current densities. The differences between the various bi-layer membranes well correspond to the FC behaviour observed in the high current range (Fig. 5) *i.e.* the increase of the FC performances corresponds to the decrease of the ohmic resistivity of the corresponding bi-layer. So, for both operating conditions, the Nafion/Nafion symmetric bi-layer exhibits the highest resistivity and the Aquivion/Aquivion bi-layer the lowest. Asymmetric materials have similar resistivities at "wet" conditions, closer to that of the Aquivion/Aquivion bi-layer.

Differently, at "dry" conditions, the (A)Aquivion/Nafion(C) assembly shows slightly lower values of both ohmic and non-ohmic contributions at high current density.

At "wet" operating conditions, the FC is fed with H₂ and O₂ both saturated with water. The water distribution in the MEA is expected to be homogeneous and the membrane water content to correspond to the equilibrium value at 100 % RH. Then, the different resistivities observed for the homogeneous bi-layers seem to correspond to the different water sorption abilities of the Nafion and Aquivion membranes. Aquivion exhibits higher IEC, conferring larger water content (*vide infra*) and so larger proton mobility.³¹ However, the mere difference between the equilibrium water contents can not explain the different behaviours and FC performances observed under "dry" conditions for the reversed orientations of the asymmetric bi-layer in the MEA. FC operation under "dry" conditions (0 % RH of both feed gases) is expected to induce heterogeneous water distribution inside the MEA. Then, the emphasizing of the differences observed between the various bi-layers at high currents strongly suggests different water repartitions inside the MEA. This implies different water transport properties for the asymmetric membrane depending on the position of the two layers with respect to the electrodes.

To summarize key results, the Aquivion symmetric bi-layer exhibits the best performances while the Nafion symmetric bi-layer the worst. The Aquivion/Nafion asymmetric membrane shows intermediate response, with better performances when the Aquivion layer is placed at the anode side. The difference between the membranes is enhanced by operating the FC under "dry" conditions.

3.2 Macroscopic measurements of water transport

Several studies attest that the PFSA membranes ability to transport water can change drastically as a function of the water content (see for example Heitner-Wirguin³³, Mauritz *et al.*³⁴, Kreuer *et al.*³⁵, and references therein). It is therefore needful to establish in advance the basic water sorption properties of the two ionomers composing the asymmetric membrane *i.e.* which material accumulates more water when free from external constraints. Fig. 7 compares sorption isotherms of single-layer Nafion[®] NRE212 and Aquivion[™] E790-05s membranes at room temperature. The water amount reported at 100 % RH corresponds to the equilibrium with liquid water and matches well to that obtained from Raman measurements carried out under the same conditions (see Fig. S1† and section 2.6). These data are used in the following (sections 3.2.1 and 3.2.2), where the water transport properties of the different symmetric and asymmetric materials are presented as a function of the water content λ . In the case of measurements carried out with the membrane submitted to an external water activity gradient, the average water content of the sample is assumed to be the equilibrium value at the water activity corresponding to the average RH value between those at the opposite sides of the sample.

Both isotherms reported in Fig. 7 exhibit the typical sigmoidal shape well described by the new dual mode sorption

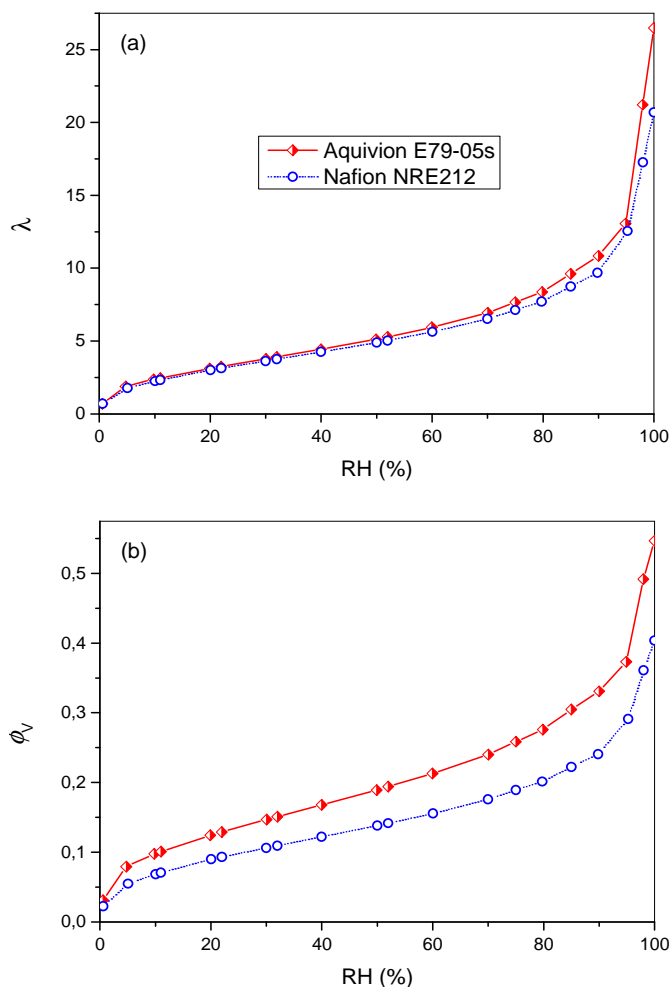


Fig. 7 Sorption isotherms of Nafion NRE212 (EW = 1100 g mol⁻¹) and Aquivion E790-05s (EW = 790 g mol⁻¹) at room temperature: (a) evolution of the water molecule number with the RH, (b) of the water volume fraction.

model of Feng⁴⁷, recently tested by Li *et al.*⁴⁸ on the vapour sorption data reported in literature for PFSA ionomers. The concave profile observed at low RHs corresponds to the sorption of strong bonding water molecules in the first hydration layer of the sulfonic ion pair. At this stage, water molecules occupy frozen spaces available in the dry ionomer network, without significant swelling strain.⁴⁸ The upward curvature at higher RHs is due to the water molecules clustering into multiple layers on the first hydration shell and inflating the hydrophilic domains. At a given RH, the water content of the membrane results from a complex interplay between the driving force for sorption, *i.e.* the solvation of ionic charges, and opposite forces due to the energy expense to expand the polymer network against its elastic resistance. Then, the almost identical sorption isotherms $\lambda = f(\text{RH})$ ($\Delta\lambda \leq 1$ for $\text{RH} \leq 90\%$, Fig. 7a) attest the similarity between the affinity of Nafion and Aquivion sulfonic groups to water as well as the presence of comparable frozen free volumes around sulfonic groups in the dry polymer network (despite the different length of the

respective side chains). The slightly larger values observed for Aquivion at the higher water activities are a hint of lower stiffness of the polymer network.

Essential to understand the different water transport properties shown by the two membranes and discussed in the following, the larger density of sulfonic groups in Aquivion corresponds to the larger water uptake at all RH in terms of percentage of dry weight taken up (or water volume fraction, Fig. 7b).

3.2.1 WATER CROSS-FLOW AT NO-CURRENT CONDITIONS. Fig. 8 reports water flows crossing the thickness of the asymmetric membrane at various hydration states, when the opposite surfaces are swept by H_{2(g)} streams with different RHs. Results are compared to those obtained with the reference materials (symmetric bi-layers) and the corresponding source (single-layer) membranes Nafion® NRE212 and Aquivion™ E790-05s. Flows are normalized on the sorption/desorption surface and on the driving force *i.e.* $\Delta\text{RH}/t$ where ΔRH is the RH difference between opposite sides and t the membrane thickness.

In agreement with the nano-phase separated morphology most widely used to understand transport properties of PFSA ionomers (see Mauritz *et al.*³⁴, Kreuer *et al.*³⁵ and references therein), the general trend observed in Fig. 8 is the increase of the water transport ability with the increase of the membrane water content. Indeed, the ratio between weak and strong bonding water molecules increases with hydration. The first hydration layer of $-\text{SO}_3^-$ groups provides a shield preventing the other molecules to interact with the acid-sites. *Alias*, the friction forces between the water molecules and the polymer phase, together with the tortuosity of the water path, decreases with the water content increase, and so the resistance to water transport.

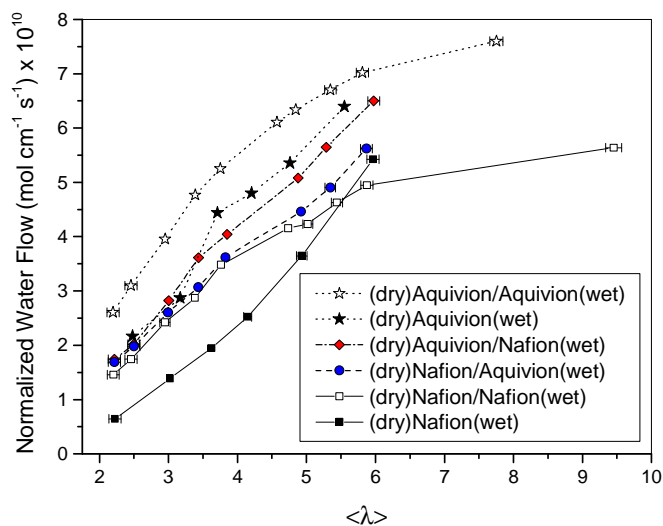


Fig. 8 Normalized water cross-flows under external RH gradient, as a function of the average membrane water content $\langle\lambda\rangle$ at room temperature: comparison between bi- (open and colourful symbols) and single-layer (black symbols) membranes. In the legend, (dry) and (wet) denote the membrane side in contact with the H_{2(g)} stream of lower and higher RH respectively. If not shown, errors are within the symbol size.

Aquivion membranes (both single- and symmetric bi-layers) exhibit the highest water flows while Nafion-based materials the lowest. Asymmetric bi-layers show intermediate values, with sensibly higher flows when the Aquivion layer is placed in contact with the less humidified hydrogen feed. Overall, these data reflect the higher water volume fraction of Aquivion at all RH values, compared to Nafion (Fig. 7b). For a given λ , Aquivion exhibits larger and/or better connected water channels through the polymer phase *i.e.* lower water transport resistance through the bulk membrane.

The lower water flows observed for single layers, compared to symmetric bi-layers of the same ionomer (either Nafion and Aquivion), as well as the decrease of this difference with the increase of the membrane hydration are the hint of surface phenomena limiting water transport.^{49,50} Indeed, it has been demonstrated that the impact of sorption/desorption limiting mechanisms on water flows, due for example to the presence of skin layers and/or to the water condensation latent heat, increases with the decrease of both membrane thickness and water content.^{51,52} The dependence of the relative importance of surface limiting phenomena on the membrane thickness is quite obvious. Interfacial mass transport resistance has to become negligible with respect to bulk resistance with the increase of the path length of water molecules across the polymer phase. Otherwise, relationships with the external RH are most usually explained by the structural and morphological rearrangement of the membrane surface. For example, recent AFM studies have shown that the surface of Nafion exhibits consistent loss of hydrophilic area at low RH.^{53,54}

A key result of flow measurements is to highlight different water transport abilities of the asymmetric bi-layer membrane depending on the positioning with respect to the external water activity gradient. As previously mentioned, higher flows are observed when the Aquivion layer is placed at the less humidified side of the cell. However, flows stay lower than those measured with the symmetric bi-layer entirely made of Aquivion. Otherwise, water flows measured with the reversed assembly (Nafion at the dry side) are almost the same as those observed with the Nafion symmetric bi-layer. The difference between the two asymmetric bi-layers increases with $\langle\lambda\rangle$. Then, water flows crossing the asymmetric membrane appear to be limited by the hydration state of the layer with the lower water sorption ability, that is Nafion.

3.2.2 ELECTROOSMOTIC DRAG. Fig. 9 reports the K_{drag} evolution with $\langle\lambda\rangle$ of the different single- and bi-layers membranes investigated here. As for water flows measured at no-current conditions (but with the opposite trend), water transport by proton dragging appears strictly related to the ionomer hydration state: K_{drag} decreases with the increase of the water molecule number and, for the same λ , is larger for Nafion containing membranes. This behavior agrees with our previous results, obtained with a large number of single-layer PFSA and hydrocarbon ionomers submitted to various experimental conditions of T, RH and I .^{14,52} However, it should be mentioned that the most of studies published by others report the opposite trend *i.e.* K_{drag} increases with the increase of the ionomer water

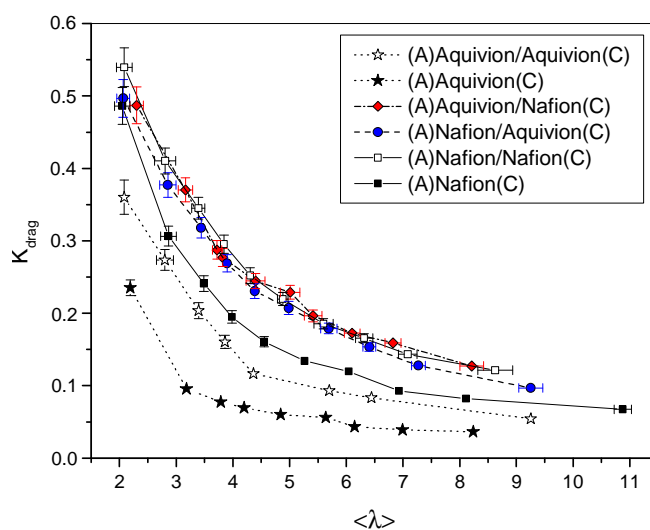


Fig. 9 Electroosmotic drag coefficient K_{drag} as a function of the average membrane water content $\langle\lambda\rangle$, at room temperature: comparison between bi- (open and colourful symbols) and single-layer (black symbols) membranes. In the legend, (A) and (C) denote the anode and the cathode respectively. If not shown, errors are within the symbol size.

content (see Ise *et al.*¹¹, Cheah *et al.*¹⁵, Kreuer *et al.*³⁵ and references therein). The invoked reason is the mobility increase of water molecules confined in the hydrophilic channels and interacting with the polymer phase. But it should be pointed out that such an explanation may lead to paradoxical conclusions when dealing with proton migration in diluted acid solutions.¹⁴ Further, the K_{drag} increase with water content would deny the proton transport mechanisms most commonly accepted for ionomers. A number of experimental⁵¹ and simulation⁵² studies attest that the motion of the excess positive charge across the membrane results from the contribution of two mechanisms: the vehicle diffusion of hydronium ions H_3O^+ , occurring at low hydration, and the Grotthus (or structural) mechanism, appearing and progressively prevailing with the increase of the sorbed water amount. The latter mechanism occurs by hydrogen-bond breaking and forming processes, without net flow of water molecules. This implies that the electroosmotic drag coefficient should stay between the limit values $0 \leq K_{\text{drag}} \leq 1$ and progressively decrease with the ionomer hydration, as actually observed in Fig. 9. More particularly, under the experimental conditions applied in this study (T_{amb}), the most of samples exhibit K_{drag} coefficients around 0.5 at the lowest water content ($\langle\lambda\rangle = 2$). This corresponds to the equivalent contribution of each mechanism to the proton migration *i.e.* half of protons moves as H_3O^+ . Lower values are observed for the Aquivion single- and symmetric bi-layers *i.e.* the membranes with the larger water volume fraction, allowing the Grotthus mechanism to prevail since the lowest hydration states. Anyhow, Fig. 9 shows that structural migration prevails increasingly from $\lambda \geq 3$ for all membranes.

Two important features in Fig. 9 are: (i) the comparability of K_{drag} measured with the asymmetric membrane differently oriented; (ii) the coincidence between these values and those

observed for the symmetric Nafion bi-layer. The common trend is the K_{drag} decrease from ~ 0.55 to ~ 0.10 in the hydration range $\lambda = 2-9$. This shows that the orientation of the asymmetric bi-layer assembly has no effect on the net electroosmotic water flow, which is instead imposed by the ionomer with the higher K_{drag} because of reasons related to the mass conservation. Indeed, at a given λ , a minimum number of solvating water molecules is needed for the proton transport across the membrane with the lower water volume fraction (Nafion), because of the higher contribution of the vehicle mechanism. Since the layers are assembled in series with respect to the charge flow, the same water flow must also cross the lower K_{drag} layer (Aquivion), the excess water being transported *via* diffusion.

As yet observed for water flows measured at no-current conditions, K_{drag} appears affected by the membrane thickness. Namely, lower electroosmotic water flows are observed for single-layers compared to the corresponding symmetric bi-layer materials (compare black and white symbols of the same shape, Fig. 9). Since this difference appears to decrease with the membrane hydration state (at least in the case of Aquivion), the same surface limiting phenomena mentioned above may be involved here *i.e.* gas/ionomer interfacial resistance to water transport. In this work, K_{drag} values are obtained from the measurement of the net water amount dragged across the membrane-electrode interfaces (see section 2.4). The experimental conditions and set-up are specifically implemented to avoid parasitic water flows due to undesired external water gradients (the appropriate method to measure the K_{drag} coefficient has been comprehensively discussed in our previous study¹⁴). Nevertheless, different interfacial transport resistances at the opposite membrane surfaces, namely water desorption faster than absorption,⁵⁰ could induce internal water gradients and consequent water back-diffusion decreasing the net water flow due to proton migration. In this case, the thicker the membrane, the lower the internal water gradient and, thus, the effect of surface limiting phenomena on the measured K_{drag} . It should be pointed out that the occurrence of different hindrances to water transport at the opposite surfaces of the membrane imply that electroosmotic drag coefficients reported in Fig. 9 may be underestimated. Anyhow, the overall trend observed, namely the K_{drag} decrease with the increase of the average membrane water content, cannot be questioned. Also, the reported K_{drag} are net values when water has to cross the membrane interface and, thus, represent the appropriate coefficient to quantify water transport in the MEA. These values, together with the flows measured at no-current conditions, are useful for the qualitative understanding of the water repartition in the working FC *via* simple phenomenological models.

3.3 Bi-layer local water content during operation

The inner water gradient crossing the asymmetric bi-layer membrane under operation is measured by *in situ* Raman microspectroscopy. Polarization data and ohmic resistivity of the single cell used for *in situ* μ -Raman are reported in Figs.

10a and b, respectively. Even if the operating conditions differ due to the specific experimental set-up (see section 2.6), results are qualitatively consistent with those obtained with the conventional cell working at representative temperature and feed gas stoichiometry (section 3.1). Better electrochemical performances, related to lower ohmic losses, are observed when the layer with the lower EW (higher IEC *i.e.* Aquivion) is placed at the anode side (compare Fig. 10 to Figs. 5 and 6).

Fig. 11 illustrates, with a selected example ($I = 222 \text{ mA cm}^{-2}$), how water concentration profiles are obtained from raw data. First, curves corresponding to the apparent Raman intensities measured for the polymer phase and sorbed water (S_{polymer} and $S_{\text{H(OH)}}$ respectively, see Fig. S1†) at different depths are convoluted separately with the instrumental spreading function.^{41,43,44} The so obtained true intensities exhibit linear gradients, progressively decreasing as the probed position moves further into the sample because of Beer-Lambert

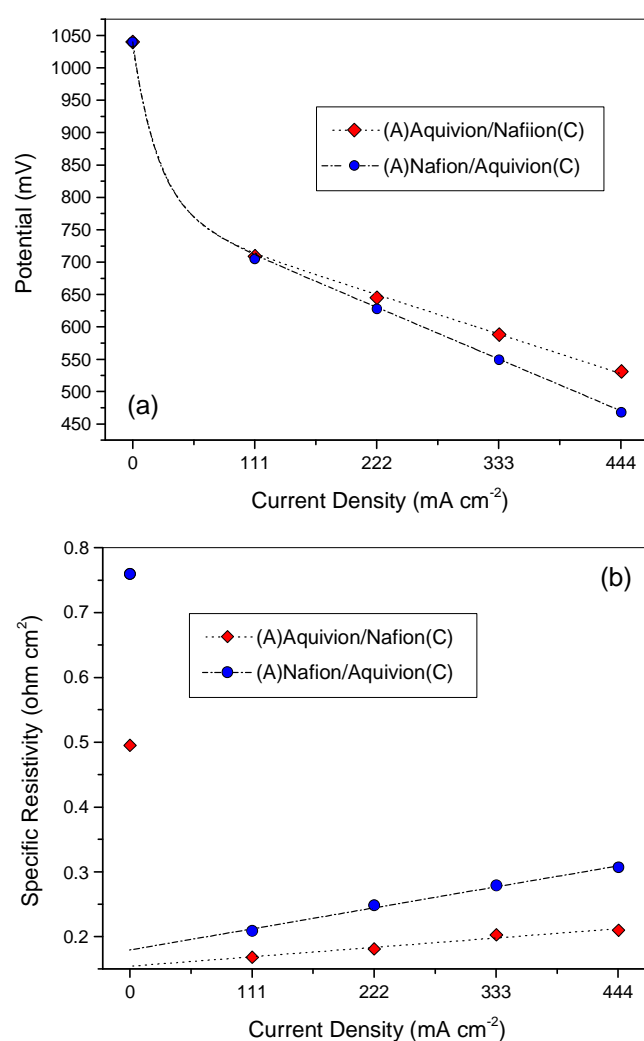


Fig. 10 (a) Polarization data and (b) specific ohmic resistivity of the PEMFC used for *in situ* Raman microspectroscopy, operated at room temperature and 50% RH for both gases. H_2/O_2 stoichiometry: 15/60. In the legend, (A) and (C) denote the anode and the cathode respectively.

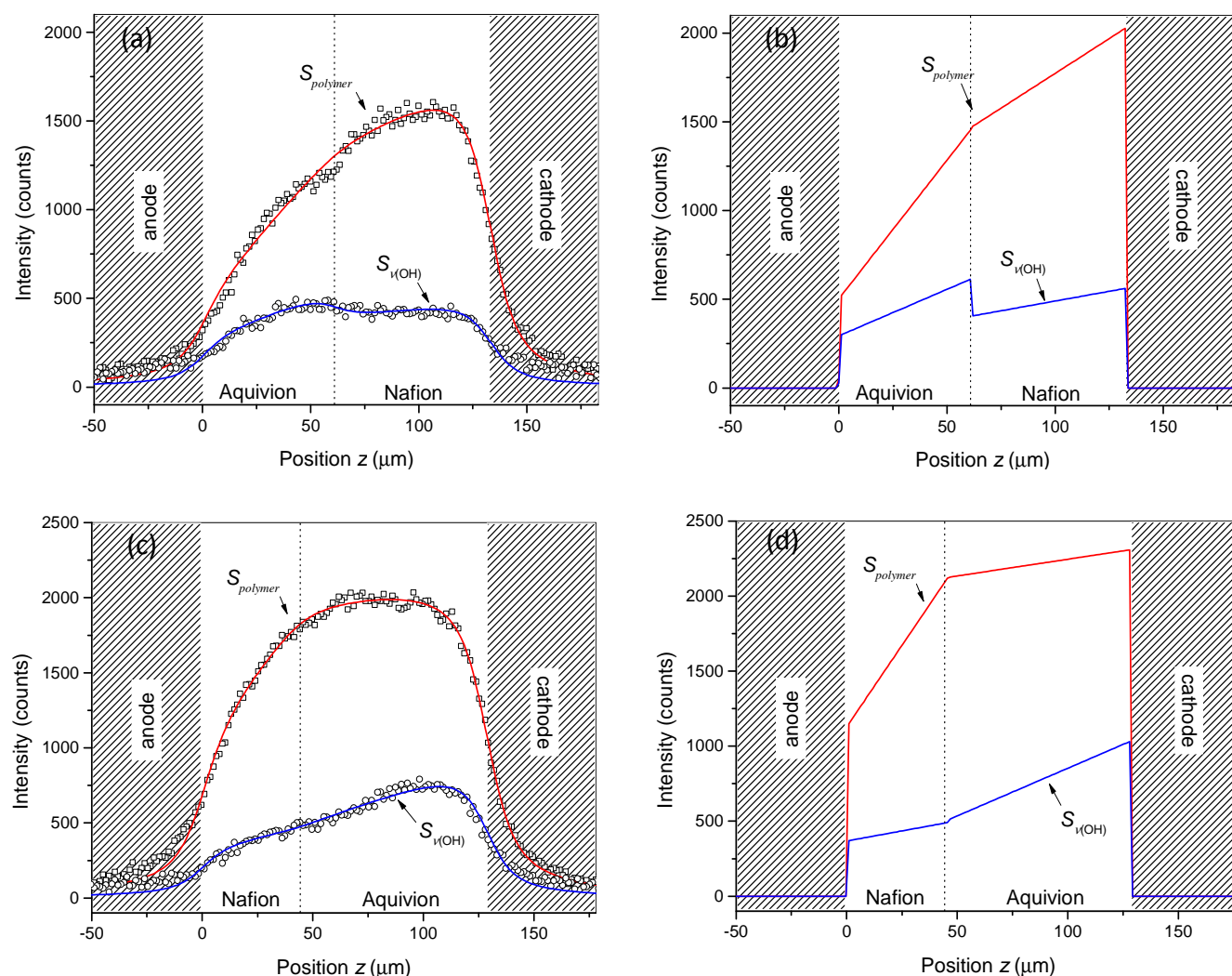


Fig. 11 Example of experimental data treatment to obtain true water concentration profiles crossing the membrane thickness during operation: (a,b) (A)Aquivion/Nafion(C) and (c,d) (A)Nafion/Aquivion(C) assembly. Symbols (left side) correspond to raw data (integrated signals of the polymer and water phases) obtained when the FC operates at $i = 222 \text{ mA cm}^{-2}$, while solid lines are the the convolution function between the true intensity profile (right side) and the instrumental spreading function.

absorption.⁴¹ Among others, these profiles are continuous *i.e.* no loss of the spectral signal is observed at the interface between the layers, showing that no disconnection occurs during operation. Then, the ratio between the water and the polymer phase signals is converted into water volume fraction and water molecule number (see eqns (5) and (6), section 2.6). Results are the complex, nonlinear depth-profiles reported in Fig. 12, showing the evolution of the membrane through-plane water content as a function of the current density delivered by the FC and of the bi-layer orientation in the MEA. The corresponding true profiles of the polymer and water phases are reported in Figs. S2 and S3 ((A)Aquivion/Nafion(C) and (A)Nafion/Aquivion(C) assemblies, respectively).[†]

The particular shapes observed in Fig. 12 for the inner water gradients can be hardly explained invoking the solely transport mechanisms of back-diffusion and electroosmosis. Apart the surface limiting phenomena highlighted by the macroscopic

measurements reported above (and often invoked in literature^{34,50,57}), further mechanisms affecting transport in the bulk appear much needed to understand such non-linear water distributions *e.g.* convective mechanism due to the presence of swelling gradients across the membrane thickness.^{31,58} The introduction of internal swelling pressure gradients as a separate driving force for water transport has previously allowed reproducing characteristic features of water concentration profiles across single-layer membranes.³¹ But, in the present case, the effect of internal pressure gradients is hardly predictable since not only related to the water activity difference at the opposite sides of the ionomer but also to the different swelling properties of the two layers solidly stacked together to build the asymmetric membrane. Thus, internal gradients of asymmetric membrane should result from the complex interplay between the different surface/bulk transport properties of the two ionomers, the different interfacial water

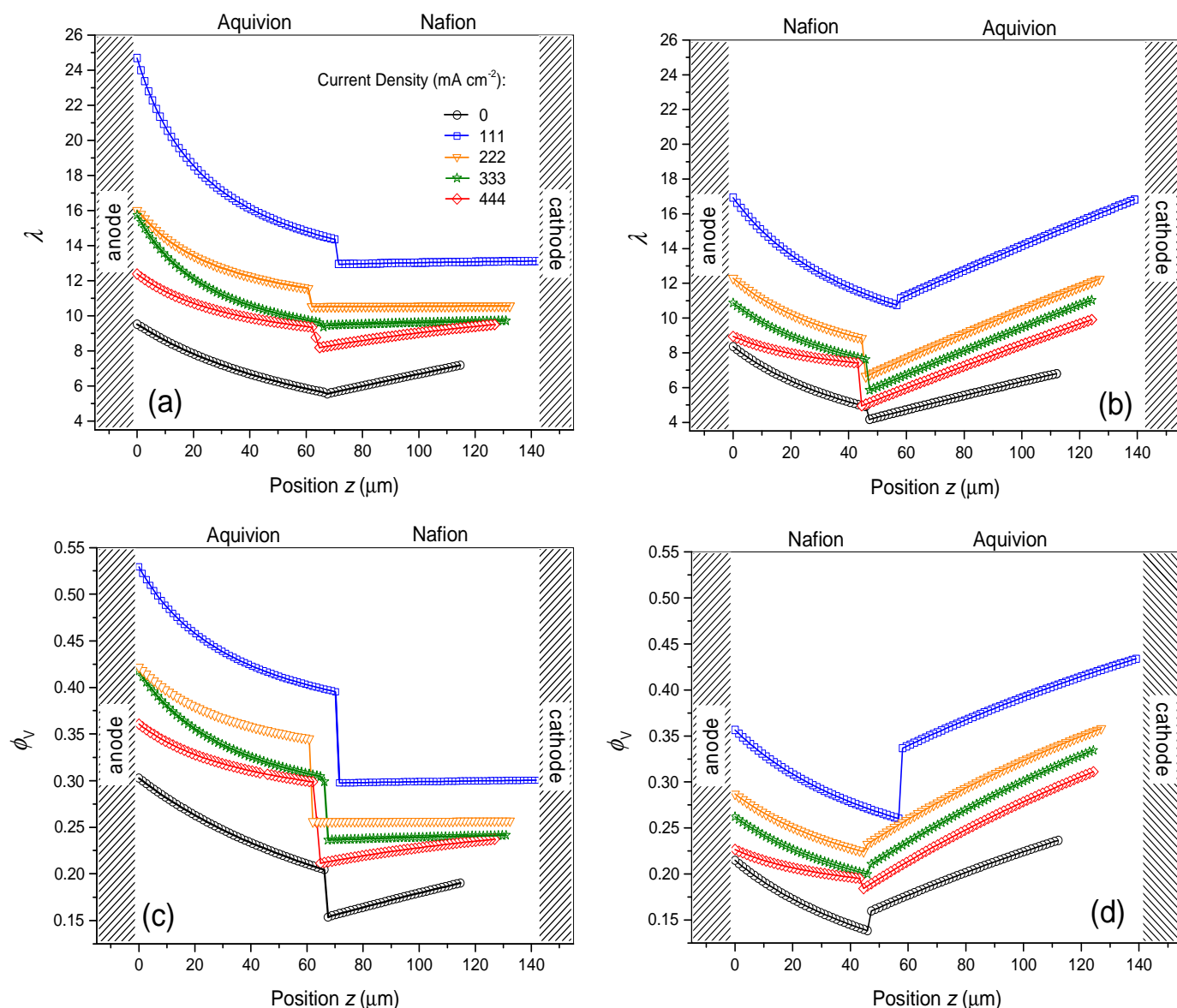


Fig. 12 Inner water concentration profiles obtained across the thickness of the heterogeneous bi-layer membrane during the FC operation: (a,b) water content is expressed as molecule number, (c,d) as volume fraction. Note that the different profiles end, at the right side, in correspondence with the interface with the gas phase and can be used to measure the actual thickness of the membrane.

transport resistances occurring at the gas/layer and layer/layer interfaces and the reciprocal hindrance to free swell. Concerning the gas/membrane interface, a last point should be also considered *i.e.* the surface modification of the polymer structure and, consequently, of the local water uptake due to the membrane-electrode assembly by hot compression.⁵⁹ Concluding, the understanding of inner water gradients across asymmetric membranes under operation is a task of the highest interest, but made particularly difficult by the simultaneous contribution of several, poorly known surface and bulk issues. This wide matter, certainly deserving further investigation and discussion, will be the subject of forthcoming works. Here below, we merely use *in situ* Raman as a probe of the local content of sorbed water, so as to establish preliminary and

qualitative relationships between the FC performances and the basic transport properties of the membrane *i.e.* back-flow and electroosmosis.

Unexpectedly, water profiles obtained at open circuit voltage (OCV) exhibit inner concentration gradients with shapes analogous to those observed during the FC operation (black symbols, Fig. 12). On the one hand, this seems to support the observations developed above *i.e.* the presence of anisotropic swelling strains independently from the external water activity while related to the multi-layer arrangement of the MEA. On the other hand, a discrepancy is observed between the average water contents of the Aquivion layer in the two assemblies. This layer exhibits higher hydration at OCV when assembled as (A)Aquivion/Nafion(C) (see also Fig. 13),

which is also attested by EIS measurements reported in Fig. 10b. Then, it should be recalled that Raman measurements at OCV are carried out after the FC operation. The membrane may not have had enough time to come back to equilibrium. Moreover, the dependence of the equilibrium water content on the membrane hydrothermal history should also be considered,⁵⁹⁻⁶¹ since the bi-layer hydration has evolved differently during the FC operation depending on the MEA orientation (*vide infra*). Anyhow, profiles recorded at OCV allow us to attest the lowest hydration of the membrane at no-current conditions.

Fig. 12 shows that, after the initial rise of the water content with the current appearance (corresponding to the beginning of

the electrochemical production of water at the cathode), the membrane hydration decreases progressively with the current increase; despite no change of the inlets RH occurs during the experiment. This behaviour is common to both MEAs. The reliability of these measurements is supported by the changes observed for the membrane thickness, which varies according to the water content measured (Fig. 12). Depending on the assembly, the overall thickness first increases from 112-115 μm at $I = 0 \text{ mA cm}^{-2}$ to 139-142 μm at $I = 111 \text{ mA cm}^{-2}$ and, then, decreases progressively down to 124-127 μm at $I = 444 \text{ mA cm}^{-2}$. Further, the observed dehydration behaviour agrees with the progressive increase of the FC ohmic resistivity with current attested by the EIS measurements (Fig. 10b). The correlation observed between local μ -Raman and macroscopic EIS measurements shows that the evolution of the membrane water content at the probed position (the middle of the active surface) qualitatively correspond to that of the most active surface.

The membrane dehydration with the increase of the current density may be surprising when considering that the FC is operated at constant gas stoichiometry and RH. Inlet reactants and water flows stay proportional to the amount of water electrochemically produced. Thus, at a given temperature, the overall concentration of water throughout the FC should be independent of the current density. Decrease of the water content could be observed in limited areas but it should correspond to the rise of the water concentration elsewhere (*e.g.* close to the gas outlets). The average water content of the membrane and the global ohmic resistivity of the MEA should stay constant. The dehydration behaviour observed in Fig. 12, concerning both MEA assemblies, does not appear to originate from the particular properties of the membranes investigated here but rather to depend on the FC operation mechanism. The increase of the water electroosmotic flow as the current density increases is usually considered to deplete water at the anode side.⁷⁻¹⁵ But this should also induce inner water gradients increasingly growing from the anode to the cathode with current,¹⁵ which is not particularly observed here. Thus, two concomitant phenomena seem to us reasonable to explain the membrane dehydration: (i) the decrease of water flows at the inlets due to pressure losses, (ii) the increase of the FC temperature because of ohmic losses and overpotentials. Despite pressure losses at the inlets are usually neglected, they may appreciably affect the average water concentration inside the cell, according to the design of the gas feed channels. When working at constant RH and stoichiometry, the increase of the current intensity delivered by the FC corresponds to the rise of the feed gases flow rate. Then, pressure drops along the channels may induce the gradual decrease of the feed gases RH from inlet to outlet with the current increase. In the present case, preliminary measurements and calculations show that water vapour pressure losses are negligible at the anode side. Otherwise, losses at the middle of the cathode side (where the depth of the channel is lower, see section 2.6) should correspond to the 5–10% decrease of the initial RH value provided at the inlet when current density attains 444 mA cm^{-2} .

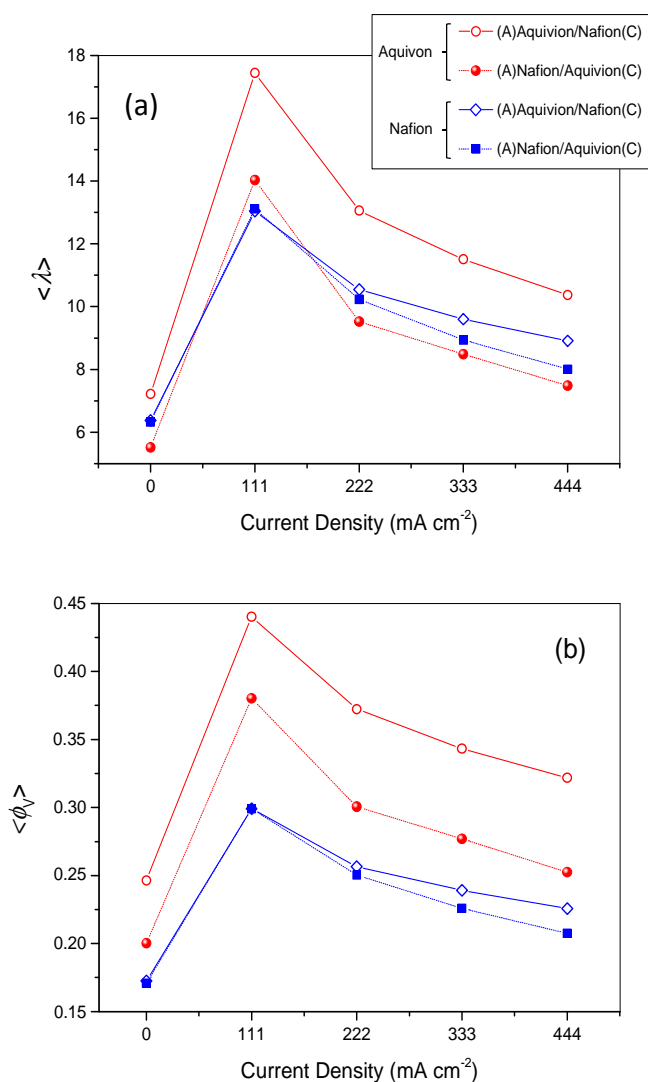


Fig. 13 Evolution of the average water content of the different layers with the current density delivered by the FC: (a) water molecule number and (b) water volume fraction. Red and blue symbols refer to the Aquivion and Nafion layers respectively. Open symbols refer to the assembly with Aquivion at the anode side and full symbols to the reversed assembly. In the legend, (A) and (C) denote the anode and the cathode respectively.

Anyhow, even if not negligible, this loss does not appear to explain alone the overall dehydration observed in Fig. 12. The gradual increment of the internal FC temperature should occur concomitantly. This increment corresponds to the decrease of the feed gases RH at the actual cell temperature and, consequently, of the membrane water content. Indeed, measurements carried out during operation show that the temperature of the bipolar plates can increase from 28 °C (ambient temperature) at $I = 111 \text{ mA cm}^{-2}$ up to 30 °C at $I = 444 \text{ mA cm}^{-2}$. In this case, the actual RH provided by the feed gases at 444 mA/cm² is 44% (instead of 50%). Anyway, the actual temperature rise at the membrane is much probably higher than 2 °C (and, so, the RH decrease larger) since the bipolar plates are made of stainless steel i.e. a poor thermal conductor. Moreover, the contribution of the water produced by the electrochemical reaction to the FC internal RH is also strongly decreased with the increase of the cell temperature.

One of the most striking results of *in situ* μ -Raman is to highlight the different dehydration behavior of the MEA depending on the bi-layer orientation. Fig. 13 compares the evolution of the average water content of each layer separately with the current density delivered by the FC, for the two assemblies. In agreement with polarization data and IES measurements (Fig. 10), the (A)Aquivion/Nafion(C) assembly exhibits the larger average water content for all currents. Interestingly, this larger hydration is mainly due to the larger water content of the Aquivion layer, the Nafion layer appearing much less affected by the MEA orientation. Otherwise, the two layers show almost the same water loss rate whatever the assembly. Considering the similarity between the $\lambda = f(\text{RH})$ sorption isotherms of Nafion and Aquivion, this behaviour supports the assumption of the FC heating as a main phenomenon contributing to the MEA dehydration.

The ability of *in situ* μ -Raman to accurately measure water contents at the micrometer scale makes this method a useful probe of the actual feed gases RH at the investigated area. Fig. 14 reports the RH evolution with current at the anode and the cathode sides, for both assemblies. RH values are obtained from the membrane water content as measured by μ -Raman at the surface swept by the hydrated gas and from the sorption isotherms reported in Fig. 7. Clearly, this implies the rough assumption of the membrane surface at the equilibrium with the gas phase, disregarding the different surface phenomena and structural modifications evoked above. Nevertheless, in this case also, the likely inaccuracy of the individual RH values does not question the general trends observed as well as the different behaviours shown by the two assemblies. The maximum value of the apparent RH, observed at $I = 111 \text{ mA cm}^{-2}$, ranges from 95.5 to 99.5% i.e. largely exceeds the hydration of feed gases at the inlets. Not surprising, the FC exhibits water accumulation in the gas feed channels at the middle of the active surface, which is the area where maximum water concentration is expected when operating in the counter-flow configuration. Overall, larger RH are observed at the anode, with maximum values attained when the Aquivion layer is placed at this side. Also, the (A)Aquivion/Nafion(C)

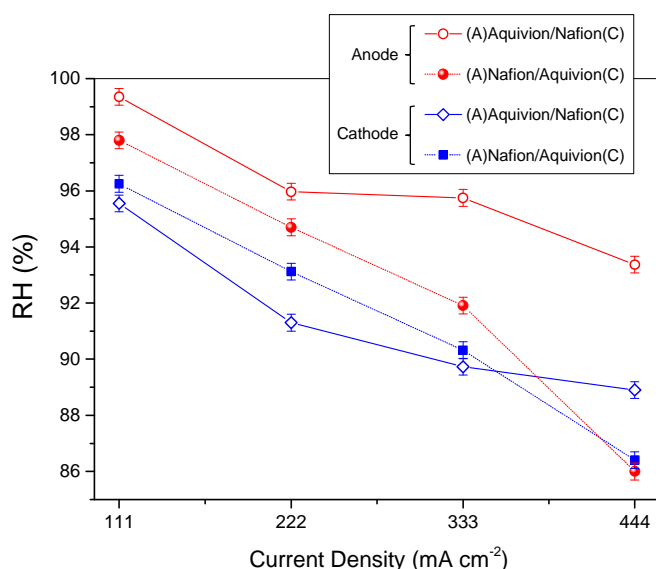


Fig. 14 Evolution of the RH in the anode (red symbols) and cathode (blue symbols) channels with the current density delivered by the FC. The probed area corresponds to the middle of the active surface. Open symbols refer to the assembly with Aquivion at the anode side and full symbols to the reversed assembly. In the legend, (A) and (C) denote the anode and the cathode respectively.

assembly shows larger difference between the RHs of the anode and cathode channels and, noteworthy, slower RH decrease with the current increase. More precisely, a decrease of ~6.5% units is observed at both sides, which would correspond to the local increase of temperature to around 29° C. The RH difference between anode and cathode stays between 4 and 6%. The reversed assembly exhibits RH decreases of 10 and 12% units at the cathode and anode sides respectively, corresponding to a local temperature increase to ~30° C. The Δ RH between the opposites sides is almost negligible (around 1.5%, but for $I = 444 \text{ mA cm}^{-2}$ where difference can no more be measured). These results definitively attest the impact of the bi-layer orientation on the water repartition at the opposite sides of the MEA. According to the water transport properties established above by *ex situ* macroscopic measurements, the (A)Aquivion/Nafion(C) assembly has improved net water-flow from the cathode to the anode, insuring better hydration of the last. Jung *et al.* have recently demonstrated the importance of adequate hydration of the ionomer in the anode AL for the effective FC working.⁶² Thus, a preliminary and qualitative relationship between water transport properties of the membrane and water repartition inside the FC is established. A more quantitative analysis would require implementing data from the middle of the FC by probing other areas closer to the gas inlets and outlets.

4 Conclusions

The fundamental understanding of coupled charge/mass transport processes as well as the detailed knowledge of specific materials response to varying operating conditions is

extremely desired to assess the FC behavior. More particularly, accurate and reliable projections of water flows through the polymer electrolyte are required to evaluate the efficiency of the PEMFC design. In this context, the understanding and management of the opposite water flows induced by diffusion, convection and electroosmotic drag across the working MEA is critical.

This work, comparing the behavior of membranes featured by through-plane symmetric and asymmetric compositions, represents a contribution to the accurate establishment of relationships between the water transport properties of the polymer electrolyte and the FC performances. First, water transport appears closely related to the hydration ability of the PFSA polymer. Because of the higher water content (related to the higher density of sulfonic groups), Aquivion™ E79-05s exhibits higher water transport by diffusion and lower electroosmotic drag compared to Nafion® NRE212. Intermediate water diffusion properties can be obtained by coupling these different materials in the bi-layer membrane, while electroosmosis remain unaffected and correspond to that of the less-hydrated ionomer, Nafion. Namely, asymmetric membranes exhibit larger water flows at no-current conditions when the Aquivion layer is placed at the cell side with the lower water concentration. Then, FC tests comparing behaviours of symmetric and asymmetric bi-layers (the last oriented differently in the MEA) confirm that increasing the water flows ratio between back-diffusion and electroosmosis has a beneficial effect on the electrochemical performances. Thus, as far as the asymmetric membranes are concerned, better performances are obtained by placing the layer with the higher hydration ability (Aquivion) at the anode side. *In situ* Raman microspectroscopy shows that this MEA configuration allows raising the average water content of the membrane under operation and, more particularly, the hydration at the interface with the anode. Proton conductivities of both the electrolyte and the anode AL are improved and the FC operation results less affected by the increase of ohmic losses with the current density. Further, the observation that the differences between the performances of the various MEA here investigated are enhanced when the FC works under “dry” conditions suggests that improved water back-flows together with limited electroosmosis also allows a better (less heterogeneous) on-plane water repartition in the cell, *i.e.* increased water content at the inlet anode side and decreased water accumulation at the outlet cathode side.

In perspective, this work highlights that water back-flows across the membrane can be improved, at a given RH, by the deposition of thin surface layers with increased IEC, placed at the FC anode side. More generally, some management of water flows can be achieved in the operating FC by using membranes with a through-plane compositional gradient. This can be particularly interesting for limiting power losses under specific working conditions and for improving those materials having the required features of durability and mechanical properties but unable to ensure adequate hydration of the MEA. Nevertheless, the results here reported do not allow us to

definitively state the interest of multi-layer PFSA electrolytes for future use in PEMFCs, since the best electrochemical performances are obtained with the homogeneous bi-layer Aquivion/Aquivion *i.e.* the membrane with the highest water back-flow and the lowest electroosmosis. Anyhow, bi-layer PFSA membranes remain excellent model materials to progress in the understanding of water transport fundamental mechanisms and relationships with the PEMFC behaviour.

For the first time, *in situ* Raman microspectroscopy has been carried out across the asymmetric bi-layer membrane during operation. The so-obtained water inner profiles exhibit high complexity and raise a number of questions about the different mechanisms and driving forces affecting the water sorption and transport across the membrane. These results emphasize that further experimental and theoretical work is needed to progress in understanding fundamental transport phenomena, namely the interplay between surface and bulk mechanisms and relationships with water management. However, *in situ* μ -Raman proves to be a unique tool to measure the actual water content of the membrane during operation and, therefore, can be used as in-time probe of the water concentration distribution along the gas feed channels upon varying working conditions. In perspective, this appears particularly useful for the effective monitoring of the FC state-of-health, since different causes of failure, *i.e.* excessive drying or flooding, lead to the same voltage drop on polarisation curves. For future works, the specific design of the FC coupled to the Raman spectrometer will be modified as to carry out experiments at representative conditions of temperature and stoichiometry, in different areas of the active surface.

Acknowledgements

This work was supported by the Agence Nationale de la Recherche (ANR, France) through the INEXTREMIS project no. ANR-10-HPAC-003.

Notes and references

^a LITEN-DEHT-LCPPEM, CEA-Grenoble, 17 rue des Martyrs, 38054 Grenoble cedex 9, France. E-mail: arnaud.morin@cea.fr; Tel: +33-4-38-78-59-86

^b IEM (Institut Européen des Membranes), UMR 5635 (CNRS-ENSCM-UM2), Université Montpellier 2, Place E. Bataillon, F- 34095, Montpellier, France. E-mail: stefano.deabate@univ-montp2.fr.fr; Fax: +33-4-67-14-91-19 ; Tel: +33-4-67-14-91-12

† Electronic Supplementary Information (ESI) available: additional figures reporting the Raman spectra of Nafion® NRE212 and Aquivion™ E79-05s soaked in water, the concentration profiles of the sorbed water and polymer phases obtained across the asymmetric bi-layer membrane during operation in the FC. See DOI: 10.1039/b000000x/

- 1 W. Schmittinger and A. Vahidi, *J. Power Sources*, 2008, **180**, 1.

- 2 N. Yousfi-Steiner, Ph. Mocotéguy, D. Candusso, D. Hissel, A. Hernandez and A. Aslanides, *J. Power Sources*, 2008, **183**, 260.
- 3 M. Ji and Z. Wei, *Energies*, 2009, **2**, 1057.
- 4 J. P. Owejan, J. J. Gagliardo, J. M. Sergi, S. G. Kandlikar and T. Trabold, *Int. J. Hydrogen Energy*, 2009, **34**, 3436.
- 5 W. Dai, H. Wang, X.-Z. Yuan, J. J. Martin, D. Yang, J. Qiao and J. Ma, *Int. J. Hydrogen Energy*, 2009, **34**, 9461.
- 6 H. Li, Y. Tang, Z. Wang, Z. Shi, S. Wu, D. Song, J. Zhang, K. Fatih, J. Zhang, H. Wang, Z. Liu, R. Abouattallah and A. Mazza, *J. Power Sources*, 2008, **178**, 103.
- 7 T. F. Fuller and J. Newman, *J. Electroanal. Soc.*, 1992, **139**, 1332.
- 8 A. Zawodzinski, J. Davey, J. Valerion and S. Gottesfeld, *Electrochim. Acta*, 1995, **40**, 297.
- 9 A. B. LaConti, A.R. Fragala and J. R. Boyack. Proceedings of the Symposium on Electrode Materials and Processes for Energy Conversion and Storage, in: J.D.E. McIntyre, S. Srinivasan, F.G. Will (Eds.), PV 77-6, *The Electrochemical Society Softbound Proceedings Series*, Princeton, NJ, 1977, p. 354.
- 10 F. Meier and G. Eigenberger, *Electrochim. Acta*, 2004, **49**, 1731.
- 11 M. Ise, K. D. Kreuer and J. Maier, *Solid State Ionics*, 1999, **125**, 213.
- 12 S. Ge, B. Yi and P. Ming, *J. Electroanal. Soc.*, 2006, **153**, A1443.
- 13 Z. Luo, Z. Chang, Y. Zhang, Z. Liu and J. Li, *Int. J. Hydrogen Energy*, 2009, **35**, 3120.
- 14 Z. Peng, A. Morin, P. Hugué, P. Schott and J. Pauchet, *J. Phys. Chem. B*, 2011, **115**, 12835.
- 15 M. J. Cheah, I. G. Kevrekidis and J. Benziger, *J. Phys. Chem. B*, 2011, **115**, 10239.
- 16 T. A. Zawodzinski, M. Neeman, L. O. Sillerud and S. Gottesfeld, *J. Phys. Chem.*, 1991, **95**, 6040.
- 17 T. A. Zawodzinski, C. Derouin, S. Radzinski, R. J. Sherman, V. T. Smith, T. E. Springer and S. Gottesfeld, *J. Electrochem. Soc.*, 1993, **140**, 1041.
- 18 S. Motupally, A. J. Becker and J. W. Weidner, *J. Electrochem. Soc.*, 2000, **147**, 3171.
- 19 J. Perrin, S. Lyonnard and F. Volino, *J. Phys. Chem. C*, 2007, **111**, 3393.
- 20 M. A. Hickner, H. Ghassemi, Y. S. Kim, B. R. Einsla and J. E. McGrath, *Chem. Rev.*, 2004, **104**, 4587.
- 21 H. Zhang and P. K. Shen, *Chem. Rev.*, 2012, **112**, 2780.
- 22 M. Marrony, J. Rozière, D. J. Jones and A. Lindheimer, *Fuel Cells*, 2005, **5**, 412.
- 23 H. Li, M. Ai, F. Jiang, H. Tu and Q. Yu, *Solid State Ionics*, 2011, **190**, 25.
- 24 J. R. Lee, J. H. Won, K. S. Yoon, Y. T. Hong and S. Y. Lee, *Int. J. Hydrogen Energy*, 2012, **37**, 6182.
- 25 C. C. Lin, W. F. Lien, Y. Z. Wang, H. W. Shiu and C. H. Lee, *J. Power Sources*, 2012, **200**, 1.
- 26 W. Li and A. Manthiram, *J. Power Sources*, 2010, **195**, 962.
- 27 M. Kamiya, M. Yoshizawa-Fujita, Y. Takeoka and M. Rikukawa, *Electrochim. Acta*, 2010, **55**, 1385.
- 28 J.-J. Woo, S.-J. Seo, S.-H. Yun, T. Xu, J. Lee and S.-H. Moon, *Electrochem. Comm.*, 2010, **12**, 148.
- 29 V. Arcella, A. Ghielmi, L. Merlo and M. Gebert, *Desalination*, 2006, **199**, 6.
- 30 A. Ghielmi, P. Vaccarone, C. Troglia, and V. Arcella, *J. Power Sources*, 2005, **145**, 108.
- 31 K. D. Kreuer, M. Schuster, B. Obliers, O. Diat, U. Traub, A. Fuchs, U. Klock, S. J. Paddison, and J. Maier, *J. Power Sources*, 2008, **178**, 499.
- 32 A. Stassi, I. Gatto, E. Passalacqua, V. Antonucci, A. S. Arico, L. Merlo, C. Oldani, and E. Pagano, *J. Power Sources*, 2011, **196**, 8925.
- 33 Heitner-Wirguin, *J. Membr. Sci.*, 1996, **120**, 1.
- 34 K. A. Mauritz, and R. B. Moore, *Chem. Rev.*, 2004, **104**, 4535.
- 35 K. D. Kreuer, S. J. Paddison, E. Spohr, and M. Schuster, *Chem. Rev.*, 2004, **104**, 4637.
- 36 P. Hugué, A. Morin, G. Gebel, S. Deabate, A. K. Sutor, and Z. Peng, *Electrochem. Comm.*, 2011, **13**: 418.
- 37 M. Hara, J. Inukai, K. Miyatake, H. Uchida and M. Watanabe, *Electrochim. Acta*, 2011, **58**, 449.
- 38 M. Hara, J. Inukai, B. Bae, T. Hoshi, K. Miyatake, M. Uchida, H. Uchida and M. Watanabe, *Electrochim. Acta*, 2012, **82**, 277.
- 39 A. Martinelli, C. Iojoiu and N. Sergent, *Fuel Cells*, 2012, **12**, 169.
- 40 S. Deabate, G. Gebel, P. Hugué, A. Morin, and G. Pourcelly, *Energy Environ. Sci.*, 2012, **5**, 8824.
- 41 S. Deabate, P. Hugué, A. Morin, G. Gebel, Y. Lanteri, Z. Peng, and A.-K. Sutor, *Fuel Cells*, 2014, in press, doi: 10.1002/fuce.201300236.
- 42 Z. Peng, P. Hugué, S. Deabate, A. Morin, and A. K. Sutor, *J. Raman Spectrosc.*, 2013, **44**, 321.
- 43 S. Deabate, R. Fatnassi, P. Sostat, and P. Hugué, *J. Power Sources*, 2008, **176**, 39.
- 44 A. Gallardo, S. Spells, R. Navarro and H. Reinecke, *J. Raman Spectrosc.*, 2007, **38**, 880.
- 45 N. J. Overall, *Analyst*, 2010, **135**, 2512.
- 46 N. Fouquet, C. Doulet, C. Nouillant, G. Dauphin-Tanguy and B. Ould-Bouamama, *J. Power Sources*, 2006, **159**, 905.
- 47 Feng, *Polymer*, 2007, **48**, 2988.
- 48 Y. Li, Q. T. Nguyen, C. L. Buquet, D. Langevin, M. Legras, and S. Marais, *J. Membr. Sci.*, 2013, **439**, 1.
- 49 P. W. Majsztrik, M. B. Satterfield, A. B. Bocarsly and J. B. Benziger, *J. Membr. Sci.*, 2007, **301**, 93.
- 50 M. B. Satterfield and J. B. Benziger, *J. Phys. Chem. B*, 2008, **112**, 3704.
- 51 D. Rivin, C. E. Kendrick, P. W. Gibson, and N. S. Schneider, *Polymer*, 2001, **42**, 623.
- 52 Z. Peng, *Thesis*, Ecole Nationale Supérieure de Chimie de Montpellier, 2012.
- 53 J. R. O'Dea, N. J. Economou and S. K. Buratto, *Macromol.*, 2013, **46**, 2267.
- 54 N. J. Economou, J. R. O'Dea, T. B. McConnaughy and S. K. Buratto, *RCS Adv.*, 2013, **3**, 19525.
- 55 T. Dippel, and K. D. Kreuer, *Solid State Ionics*, 1991, **46**, 3.
- 56 D. Seeliger, C. Hartnig, and E. Spohr, *Electrochim. Acta*, 2005, **50**, 4234.

- 57 B. Kientiz, H. Yamada, N. Nonoyama and A. Z. Weber, *J. Fuel Cell Sci. Technol.*, 2010, **8**, 011013.
- 58 K.-D. Kreuer, *Solid State Ion.*, 2013, **252**, 93.
- 59 A. Kusoglu, S. Savagatrup, K. T. Clark and A. Z. Weber, *Macromol.*, 2012, **45**, 7467.
- 60 G. Alberti, R. Narducci, and M. Sganappa, *J. Power Sources*, 2008, **178**, 575.
- 61 A. K. Sutor, P. Huguet, A. Morin, G. Gebel, T. S. Le and S. Deabate, *Fuel Cells*, 2012, **12**, 162.
- 62 C.-Y. Jung and S.-C. Yi, *Electrochem. Comm.*, 2013, **35**, 34.